



In-situ catalytic decomposition of emitted ammonia from municipal solid waste gasification by Ni–M bimetallic catalysts supported on sewage sludge-derived biochar

Xueyu Ding¹ · Yaji Huang¹ · Xinxin Dong¹ · Jiaqi Zhao¹ · Mengzhu Yu^{1,2} · Xinqi Tian¹ · Jinlei Li¹ · Xuewei Zhang¹ · Yuxin Li¹ · Zekun Wei¹

Received: 28 September 2022 / Revised: 6 November 2022 / Accepted: 22 November 2022 / Published online: 17 February 2023
© Zhejiang University Press 2023

Abstract

Gasification technology can effectively realize energy recovery from municipal solid waste (MSW) to reduce its negative impact on the environment. However, ammonia, as a pollutant derived from MSW gasification, needs to be treated because its emission is considered harmful to mankind. This work aims to decompose the NH₃ pollutant from MSW gasification by an in-situ catalytic method. The MSW sample is composed of rice, paper, polystyrene granules, rubber gloves, textile and wood chips. Ni–M (M=Co, Fe, Zn) bimetallic catalysts supported on sewage sludge-derived biochar (SSC) were prepared by co-impregnation method and further characterized by X-ray diffraction, N₂ isothermal adsorption, scanning electron microscopy, transmission electron microscopy and NH₃ temperature programmed desorption. Prior to the experiments, the catalysts were first homogeneously mixed with the MSW sample, and then in-situ catalytic tests were conducted in a horizontal fixed-bed reactor. The effect of the second metal (Co, Fe, Zn) on the catalytic performance was compared to screen the best Ni-M dual. It was found that the Ni–Co/SSC catalyst had the best activity toward NH₃ decomposition, whose decomposition rate reached 40.21% at 650 °C. The best catalytic performance of Ni–Co/SSC can be explained by its smaller Ni particle size that facilitates the dispersion of active sites as well as the addition of Co reducing the energy barrier for the associative decomposition of NH species during the NH₃ decomposition process. Besides, the activity of Ni–Co/SSC increased from 450 °C to 700 °C as the NH₃ decomposition reaction was endothermic.

Keywords Ammonia decomposition · Municipal solid waste · Gasification · In-situ catalysis · Ni-based catalyst · Biochar

Introduction

The production amount of municipal solid waste (MSW) in China has increased sharply due to the accelerating urbanization process and living standard improvement. The total MSW production has increased from 31.3 million tons in 1980 to 235 million tons in 2020 and is estimated to reach 480 million tons in 2030 [1], which puts great

pressure on its treatment. The MSW treatment methods currently include incineration, landfill, and composting [2–4], of which incineration is the mainstream treatment approach at present for its versatile applications in electricity and heat generation. However, disadvantages such as low energy utilization, toxic dioxin production and heavy metal emission [5–7] derived from incineration have driven researchers to find supplementary or substitute treatment methods. Gasification, an effective technology for waste-to-energy (WTE) concept [8] that thermally converts MSW into gaseous products, can effectively improve the energy recovery rate and control large-scale pollution. Therefore, it has become increasingly popular in the field of solid waste treatment [8–10]. Currently, the commonly used gasification mediums for waste gasification are air, O₂, H₂O, CO₂, etc. Among them, using CO₂ as the gasification medium can produce more CO, which has received more attention in recent years. As the main component of synthesis gas, carbon monoxide is an important

✉ Yaji Huang
heyjy@seu.edu.cn

¹ Key Laboratory of Energy Thermal Conversion and Control of Ministry of Education, School of Energy and Environment, Southeast University, Nanjing 210096, China

² Department of Transdisciplinary Science and Engineering, School of Environment and Society, Tokyo Institute of Technology, Yokohama, Kanagawa 2268503, Japan

raw material for the synthesis of a series of basic organic chemicals and intermediates. The usage of CO_2 as a gasification medium can also effectively consume CO_2 in industrial flue gasses, enabling the fueling of CO_2 and the recycling of carbon. Nevertheless, MSW naturally contains nitrogen and part of it is inevitably transformed into ammonia during the gasification process [11, 12], which is detrimental to equipment due to its corrosion characteristics. Besides, NH_3 is also widely recognized as the precursor of NO_x which is harmful to the ecological environment and human health [13]. Hence, the ammonia emitted during MSW gasification must be treated to reduce its negative environmental impact as well as improve the gas product quality to meet end-use needs.

Currently, common methods used for removing NH_3 from the gas phase include solid adsorption, catalytic decomposition, electrochemical treatment and biological techniques. Among the above methods, solid adsorption is conventionally applied for low-temperature NH_3 removal. Electrochemical treatment presents several issues, such as complex mechanisms and significant electrical losses. Moreover, the widespread utilization of biological treatment faces great challenges, as it is time-consuming due to its low efficiency. The catalytic decomposition is more suitable in high-temperature environments [14], which matches the gasification conditions that usually proceed under high temperature. In research of catalytic decomposition of NH_3 , the core part is the development of efficient and stable catalysts. At present, most research on metal catalysts is centered on Ni, Fe and Ru active components [12, 15, 16], among which Ru possesses the most satisfying activity toward NH_3 decomposition. However, its wide application is restricted due to its relatively high cost [17–19]. The catalytic activity of Fe is lower than that of ruthenium- and nickel-based catalysts, although it is easily accessible [20]. Comprehensively, Ni-based catalysts are more promising, as they achieve a good balance between activity and cost. Hence, it is economic and feasible to employ Ni-based catalysts for the catalytic decomposition of NH_3 during MSW gasification [21–23].

Apart from active components, Ni-based catalysts are also composed of supports and promoters. Structurally, the catalyst support generally plays a role in dispersing the active components as well as improving the stability, which has a significant impact on NH_3 decomposition performance. Traditional catalyst supports include carbon-based materials, metal oxides and molecular sieves, among which carbon-based materials are a group of attractive and promising substrates due to their high specific surface area and favorable thermal stability [24–26]. A lot of precursors can be manufactured into carbon materials such as biomass, plastics, tires and sewage sludge. As a massive pollutant, the disposal and utilization of sewage sludge has recently been under the spotlight [27]. The preparation of biochar from

sewage sludge pyrolysis is receiving considerable attention because it is applied versatily in many fields, such as aqueous pollutant absorption and catalysis or catalyst support, due to its large surface area, well-developed pores, rich functional groups and original metal elements [28]. However, the exposed literature on the utilization of sewage sludge-derived biochar (SSC) as a catalyst support is scarce, which leaves room for us to conduct systematic research.

As a promoter, it is of great importance to enhance the activity of Ni-based catalysts [29, 30]. Boisen et al. [31] compared the adsorption energy of NH_3 on several metal surfaces during NH_3 decomposition and found that they are in the following order: $\text{Ni} < \text{Co} < \text{Ru} < \text{Fe} < \text{Mo}$. Thus, it can be theoretically predicted that the NH_3 decomposition activity can be enhanced when combining another metal such as Co, Fe and Mo with Ni to form bimetallic catalysts. However, it was found that the functional tuning and catalytic activity of Mo–X catalysts are largely limited by the large miscibility gap present in the binary alloy. Hence, the usage of Co and Fe as the secondary metals should be the focus of future research. Wu et al. [32] synthesized a series of Ni, Co and Ni–Co catalysts via the co-impregnation method and found that Ni–Co bimetallic catalysts presented better catalytic activity toward NH_3 decomposition than single Ni or Co metal catalysts. Although researchers have made great advances in NH_3 catalytic decomposition, a relevant investigation focusing on the process of MSW gasification is still worthwhile considering the complexity of MSW composition and its gasification process. Unlike the conventional gas phase treatment, in-situ catalytic decomposition of NH_3 is a new technology that premixes the MSW sample with catalyst and simultaneously causes the gasification of MSW and catalytic decomposition of emitted NH_3 , which has no additional requirements for the treatment unit and facilitates the simplification of the process [33].

In the present work, the preparation procedure of SSC supported Ni–M (M=Co, Fe, Zn) bimetallic catalysts and their activity for in-situ NH_3 decomposition during the MSW gasification process were reported. The catalysts were characterized by a series of techniques such as X-ray diffraction (XRD), N_2 isothermal adsorption, scanning electron microscopy (SEM), transmission electron microscopy (TEM) and NH_3 temperature programmed desorption (NH_3 -TPD). The effect of the added promoter was compared, and the reaction temperature on the NH_3 decomposition performance was investigated. This work was initially intended to provide a solution for NH_3 pollution control and treatment in the solid waste disposal field. The novelty lies not only in the usage of SSC as a catalyst support obeying the concept of “waste to value” but also in the practice of in-situ catalysis to simplify the process.

Experiment

Materials

The MSW sample employed in this study comprised six components, including rice, paper, polystyrene granules, rubber gloves, textile and wood chips, with a mass percentage of each component being 50%, 15%, 10%, 10%, 10% and 5%, respectively. The proximate and ultimate analyses of each component are listed in Table 1.

The sewage sludge was obtained from a local sewage treatment plant. The Nickel acetate tetrahydrate ($\text{Ni}(\text{CH}_3\text{COO})_2 \cdot 4\text{H}_2\text{O}$, Analytical Reagent), cobalt chloride hexahydrate ($\text{CoCl}_2 \cdot 6\text{H}_2\text{O}$, AR), iron nitrate nonahydrate ($\text{Fe}(\text{NO}_3)_3 \cdot 9\text{H}_2\text{O}$, AR) and zinc nitrate hexahydrate ($\text{Zn}(\text{NO}_3)_2 \cdot 6\text{H}_2\text{O}$, AR) were purchased from Sinopharm Chemical Reagent Co., Ltd (Shanghai, China). Gases including N_2 , CO_2 and H_2 were ordered from Shangyuan Industrial Gas Co., Ltd (Nanjing, China).

Catalyst preparation

The SSC was obtained by the pyrolysis method, as shown in Fig. 1a. Specifically, the newly acquired sewage sludge was first dried in an oven at 105 °C for 12 h and then crushed to particles with diameters of 180–250 μm for further use. Subsequently the sludge particles were placed in a temperature-programmed fixed-bed furnace for pyrolysis. The whole pyrolysis process was carried out at 600 °C for 2 h with a N_2 flow of 0.5 L/min and eventually the residue was collected as SSC.

The SSC supported catalysts were prepared by the co-impregnation method as depicted in Fig. 1b. A typical preparation process mainly includes four steps: co-impregnation, drying, calcination and reduction. The SSC material was first added into a solution of mixed $\text{Ni}(\text{CH}_3\text{COO})_2 \cdot 4\text{H}_2\text{O}$ and a second metal salt ($\text{CoCl}_2 \cdot 6\text{H}_2\text{O}$, $\text{Fe}(\text{NO}_3)_3 \cdot 9\text{H}_2\text{O}$, $\text{Zn}(\text{NO}_3)_2 \cdot 6\text{H}_2\text{O}$). The mixture was stirred

for 2 h and then placed in a water bath at a constant temperature of 60 °C for 4–5 h to ensure adequate impregnation. After being dried in an oven at 110 °C overnight, the catalyst precursor was calcined in a tube furnace at 450 °C under a N_2 atmosphere for 4 h and was further grinded into powder shape. Finally, the as-prepared catalyst was reduced at 450 °C for 3 h under a H_2 atmosphere. Four types of Ni-based catalysts were prepared in all and the designed Ni content and second metal content were 15% and 5% (in weight), respectively (Table 2). To facilitate the expression, the catalysts were recorded as Ni/SSC, Ni–Co/SSC, Ni–Fe/SSC, and Ni–Zn/SSC.

Catalyst characterizations

The crystal structure and physical phase analysis of the catalysts were detected by XRD on a SmartLab-3KW apparatus (RIKEN, Saitama, Japan) with Cu $K\alpha$ radiation ($\lambda=0.15406$ nm) operating at a voltage of 40 kV and current of 40 mA. The catalyst samples were scanned at a rate of 10°/min from $2\theta=5$ to 90° at a step of 0.02°. The particle size of the catalyst was calculated using the Debye–Scherrer equation, as shown in Eq. (1), where D (nm) is the particle size, K is the Scherrer constant, γ is the X-ray wavelength ($\lambda=0.15406$ nm), B (rad) is the half-height width of the diffraction peak, and θ (°) is the Bragg diffraction angle [34].

$$D = \frac{K\gamma}{B\cos\theta} \quad (1)$$

The microstructural properties of the catalysts were determined via N_2 isothermal adsorption at –196 °C using a Mike TriStar II 3020 analyzer (Micromeritics, Norcross, GA, USA). The specific surface area was calculated by Brunauer–Emmett–Teller (BET) method and the pore size distribution was acquired by Barrett–Joyner–Halenda (BJH) method.

TEM was used to observe the distribution state of the loaded metal on the support, which was analyzed by a Tecnai

Table 1 Proximate and ultimate analyses of the MSW components

Sample	Proximate analysis (% ad*)			Ultimate analysis (% ad*)				
	Moisture	Volatile	Ash	C	H	O	N	S
Rice	13.1	77.12	0.41	39.42	6.58	50.02	1.20	0.09
Paper	10.05	76.78	0.41	45.31	6.10	45.99	0.18	0.16
Plastic	0.01	99.77	0.01	91.62	7.61	1.54	0.09	0.02
Rubber	0.90	91.62	5.50	77.35	8.79	5.98	6.78	0.78
Textile	5.73	86.98	0.24	42.30	6.19	50.37	0.25	0.06
Wood Chips	18.31	68.79	1.40	41.94	5.48	42.69	0.18	0.04
MSW	9.64	81.35	0.91	49.73	6.73	39.83	1.343	0.15

*Air dried basis

MSW municipal solid waste

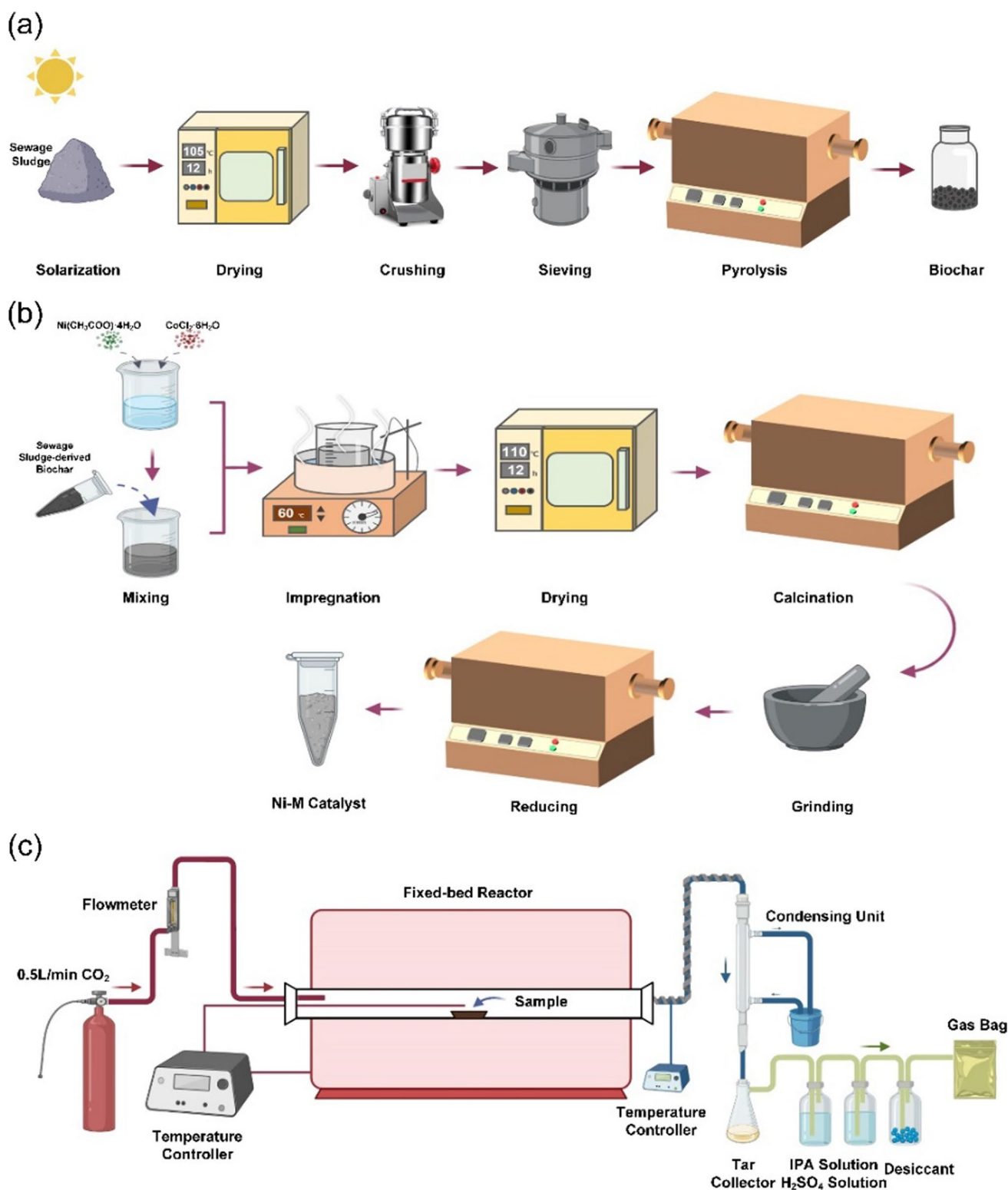


Fig. 1 Schematic diagram of (a) sewage sludge pyrolysis, (b) catalyst preparation, and (c) the fixed-bed gasification reactor

G2 F20 field emission transmission electron microscope (FEI, Hillsboro, OH, USA) with an accelerating voltage of 200 kV, a point resolution of 0.24 nm and a line resolution

of 0.14 nm. The surface morphology and element dispersion of the catalyst were observed by a S4800 (Hitachi, Japan) cold field emission SEM operating at 5.0 kV.

Table 2 Nominal composition of the four catalysts

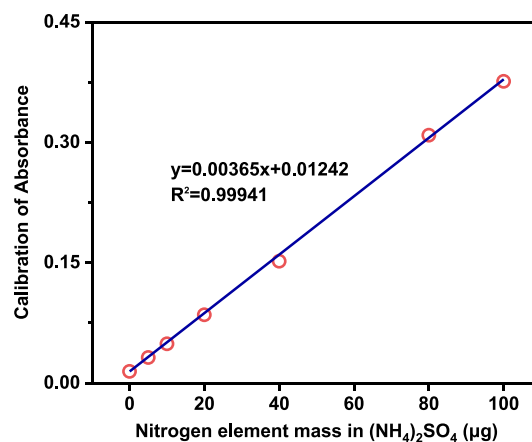
Catalyst sample	Composition (% in weight)		
	Ni	Second metal	SSC support
Ni/SSC	20	–	80
Ni–Co/SSC	15	5	80
Ni–Fe/SSC	15	5	80
Ni–Zn/SSC	15	5	80

SSC sewage sludge-derived biochar

NH₃-TPD was conducted on a TP-5080 chemisorption instrument (Tianjin, China) to elucidate the NH₃ desorption behavior associated with NH₃ decomposition-related species over catalysts. Typically, the appropriate amount of catalyst (100 mg) sample was heated to 300 °C under He flow, kept for 1 h and further cooled to 100 °C. Then, after adsorption of NH₃ at 100 °C for 30 min to saturation state, He was purged into and the temperature was increased from 50 °C to 800 °C at a rate of 10 °C/min to complete the desorption process.

Catalyst testing

The experimental system of in-situ catalytic decomposition of NH₃ from MSW gasification in this study is schematically shown in Fig. 1c. The CO₂ gasification reagent was provided by a gas cylinder with its flow rate controlled by a flowmeter. The horizontal reactor with a length of 1000 mm and inner diameter of 80 mm was heated by an electric heating rod with a temperature adjustment range from 30 °C to 1300 °C. The heating rate and reaction temperature were adjusted by a temperature controller. The pipeline connecting the reactor outlet and the condenser was wrapped with heating tape, which was maintained at 200 °C during the gasification process to prevent tar condensing and blockage in the pipeline. In a typical case, prior to the test, CO₂ was first purged into the reactor for 30 min to expel air from the system. When the reactor was heated to the desired temperature under 0.5 L/min CO₂ flow, a crucible with the mixture of MSW sample and the reduced catalyst (5 g each) was introduced into the reactor and gasified continuously for 20 min. After cooling to room temperature, the crucible was extracted from the reactor, and the residue inside was collected and sealed in plastic bags. The tar fraction was condensed by ice water in a vertical spherical condenser and further absorbed by 150 mL isopropanol alcohol prior to gas collection. Afterwards, the emitted NH₃ was absorbed by a 100 mL H₂SO₄ solution with a concentration of 0.1 mol/L. The rest of the gas products of MSW gasification were finally collected by a gas bag and further analyzed by a gas chromatograph (GC 2018, Shimadzu, Japan).

**Fig. 2** Standard curve of nitrogen element mass vs. absorbance

For NH₃ quantification, the absorbed H₂SO₄ solution was analyzed through Nessler's reagent method [35]. Generally, 1.0 mL of Nessler's reagent was added to 0.5 mL of absorbed H₂SO₄ solution. The liquid mixture was then subjected to an ultraviolet spectrophotometer (Lambda365, PerkinElmer, Waltham, MA, USA) at a wavelength of 420 nm to determine the nitrogen element mass in 0.5 mL absorbed H₂SO₄ solution, which was calculated based on the pre-measured standard curve, as shown in Fig. 2. The obtained nitrogen element mass can be further used to calculate the total emitted NH₃ from MSW gasification according to Eq. (2). The ratio of the nitrogen mass in NH₃ to the total nitrogen in the MSW sample was calculated according to Eq. (3), where *m* (mg) is the nitrogen element weight in the emitted NH₃, *α* is the absorbance and *m*_{ad} (mg) is the nitrogen element weight in the emitted NH₃ after adding catalyst under the same working conditions. The performance of the catalyst was evaluated by the decomposition rate of NH₃ (*η*), which was calculated according to Eq. (3)

$$m = \frac{100}{0.5 \times 1000} \times \frac{\alpha - 0.01242}{0.00365} \quad (2)$$

$$\eta = \frac{m - m_{ad}}{m} \times 100\% \quad (3)$$

Results and discussion

XRD and N₂ isothermal adsorption–desorption analysis

The XRD patterns in Fig. 3 can reflect the crystal structure and physical phase of the SSC sample and the changes after loading Ni, Co, Fe and Zn on this support.

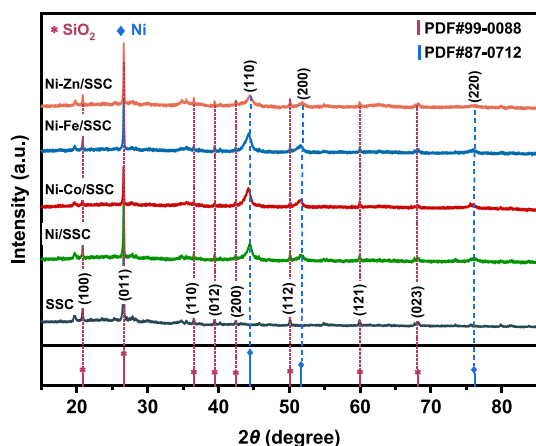


Fig. 3 XRD patterns of SSC support, Ni/SSC and Ni-M/SSC catalysts. XRD X-ray diffraction, SSC sewage sludge-derived biochar

Table 3 Microstructural parameters of SSC support and reduced Ni/SSC and Ni-M/SSC catalysts

Sample	Surface area (m ² /g)	Pore volume (cm ³ /g)	Average pore size (nm)	Ni particle size (nm)
SSC	56.33	0.13	8.73	–
Ni/SSC	172.36	0.19	4.31	10.4
Ni-Co/SSC	116.60	0.20	6.46	8.4
Ni-Fe/SSC	131.18	0.22	6.45	8.6
Ni-Zn/SSC	163.81	0.18	3.89	9.6

Multiple diffraction peaks corresponding to quartz (SiO₂) at $2\theta=20.86^\circ$, 26.64° , 36.55° , 39.47° , 42.45° , 50.14° , 59.96° and 68.14° can be observed in the SSC sample, which are attributed to the (100), (011), (110), (012), (200), (112), (121) and (203) crystal planes of SiO₂ (PDF#99-0088). Furthermore, after loading Ni, Ni-Co, Ni-Fe and Ni-Zn,

the four catalysts show similar XRD patterns to the SSC support. All the catalyst samples contain the characteristic peaks of SiO₂, indicating that the structure of the SSC support was maintained in the catalyst and was not heavily affected by the loading metal. In addition, three new peaks emerged on the basis of SSC diffraction peaks at $2\theta=44.35^\circ$, 51.74° and 76.23° . They are typical diffraction peaks of metallic Ni, which correspond to the (110), (200) and (220) crystal planes (PDF#87-0712), implying that the active Ni species were successfully loaded on the SSC support by reduction. Moreover, the four catalysts showed similar diffraction peaks even with different promoters. However, the diffraction peaks ascribed to Zn, Fe and Co are absent in the XRD patterns, possibly due to their high dispersion in the catalyst or forming bimetallic alloys with high dispersion [36]. The Ni particle size calculated according to Debye–Scherrer equation is listed in Table 3 [34]. As can be seen, the Ni particle sizes for the bimetallic catalysts all decrease after adding the second metal, which is specifically in the order of Ni-Co/SSC < Ni-Fe/SSC < Ni-Zn/SSC < Ni/SSC. It is noted that Ni-Co/SSC exhibits a smaller particle size than those of other catalysts, implying that the Co additive promotes the dispersion of Ni on the SSC support. According to some studies, the high dispersion of active sites is beneficial to enhance the NH₃ catalytic decomposition performance [37, 38].

The microstructures of the prepared SSC support and reduced Ni/SSC and Ni-M/SSC catalysts were characterized by N₂ adsorption–desorption, and the isotherms are shown in Fig. 4a. According to the classification of the International Union of Pure and Applied Chemistry, the adsorption isotherms of SSC, Ni-Co/SSC and Ni-Fe/SSC accord well with type IV isotherms with H3-type hysteresis loops, while the isotherms of Ni/SSC and Ni-Zn/SSC present typical type IV shapes with H2 hysteresis loops. The hysteresis loop in the isotherms indicates the capillary coalescence phenomenon.

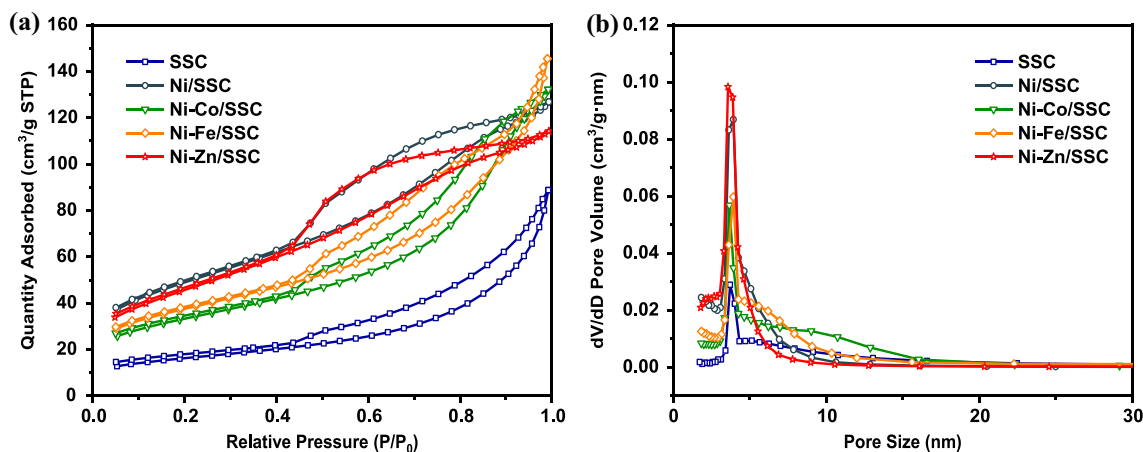


Fig. 4 (a) N₂ adsorption–desorption isotherms, and (b) pore size distribution of SSC support and reduced Ni/SSC and Ni-M/SSC catalysts

This means that the SSC support and catalysts are mainly mesoporous, and slit pores are formed by the accumulation of lamellar particles [39]. In the range of lower relative pressure, the N_2 adsorption capacity of the samples is weak due to monolayer adsorption. As the pressure increases to a certain level, the adsorption amount increases sharply due to multilayer adsorption. The pore size distribution obtained from the isotherms is shown in Fig. 4b. It can be seen that the pore size of five samples are mostly centered at around 3 nm, indicating the mesoporous characteristics of the samples. From Table 2, it can be observed that the surface area of the four catalysts is larger than that of the SSC support, which is caused by the development of micropores in the catalyst after metal addition [38]. Moreover, the surface area of bimetallic catalysts (such as Ni–Co/SSC) is smaller than that of a single metal catalyst (Ni/SSC), as the addition of a promoter might block some of the catalyst pore channels. Besides, the pore volume of catalysts also increases to some extent after metal loading. Finally, the average pore size of the five samples is in the range of 2–10 nm, indicating the mesoporous nature of the samples [9]. This is in good agreement with the results predicted by the N_2 adsorption isotherms in Fig. 4a.

TEM and SEM analysis

To further intuitively observe the morphological structures and distribution state of loading metal on the SSC support, the catalyst samples were characterized by TEM and SEM and the results are shown in Figs. 5 and 6. The TEM images of the four catalysts show that the particle size of the Ni–Co/SSC catalyst is significantly smaller than that of the other three catalysts while Ni/SSC presents the largest Ni particle size, which is consistent with the results calculated by XRD in Table 3. This phenomenon further confirms that the addition of the second metal promotes the dispersion of the active sites [40].

From the SEM image of SSC presented in Fig. 6a, it can be observed that the surface morphology of SSC is roughly

smooth and dense, displaying an irregular lamellar structure. Part of the SSC surface was destroyed and numerous particles of different sizes were scattered sporadically on the carbon layer surface, which resulted in a rough and irregular surface morphology. After loading the metal particles, it can be seen from Fig. 6b that the metal particles are attached to the lamellar SSC support surface with slight agglomeration. The overall morphology of the catalyst is relatively rough with little pore structure. The fresh Ni–Co/SSC catalyst was further characterized via element mapping, from which the element distribution over the catalyst can be seen (Fig. 6d–f). It can be noted that apart from the main element in SSC support (Si), the loaded Ni and Co elements can also be observed distinctly with uniform distribution on the support in the catalyst. The Si element from mapping characterization agrees well with the results of Fig. 3 that the main material of SSC is SiO_2 . Fig. 6c provides the SEM image of the spent Ni–Co/SSC catalyst. It can be noticed that the pore structure is obviously much more abundant after the catalytic gasification process, which may be due to a series of reactions between the carbon of SSC and the gasification medium CO_2 to activate it, thus changing its pore structure [28].

NH_3 -TPD analysis

Figure 7 displays the NH_3 -TPD results of SSC, Ni/SSC and Ni-M/SSC. It can be seen that the NH_3 -TPD curve of Ni/SSC shows three distinct desorption peaks at 188.2 °C, 395.8 °C and 600.7 °C, which correspond to the weak, moderate and strong acidic sites of the catalyst, respectively. Related studies have demonstrated that the two desorption peaks appearing at 100–200 °C and 300–500 °C correspond to weak and strong adsorption of NH_3 , respectively. The high-temperature peak (>500 °C) corresponds to the associative decomposition of NH species [37]. In contrast, the NH_3 -TPD curve of SSC only presents two desorption peaks at 190.1 °C and 400.5 °C with no high temperature peaks. This also indicates that the metal loaded on the SSC support

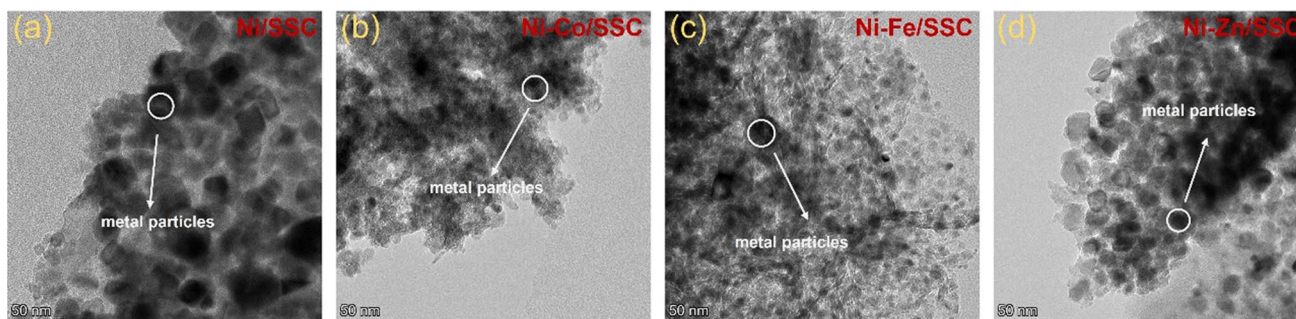


Fig. 5 TEM images of fresh reduced catalysts (a) Ni/SSC, (b) Ni–Co/SSC, (c) Ni–Fe/SSC, and (d) Ni–Zn/SSC. TEM transmission electron microscopy

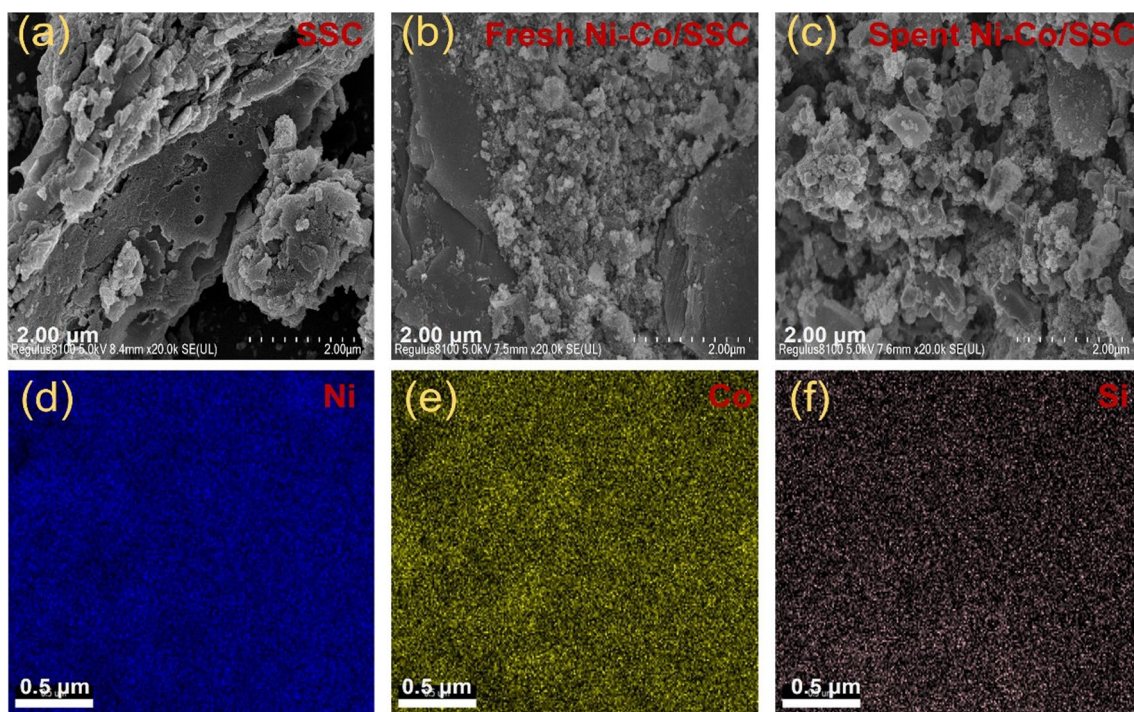


Fig. 6 SEM images of (a) SSC, (b) fresh Ni–Co/SSC, (c) spent Ni–Co/SSC, and SEM mapping images of fresh Ni–Co/SSC (d–f). SEM scanning electron microscopy

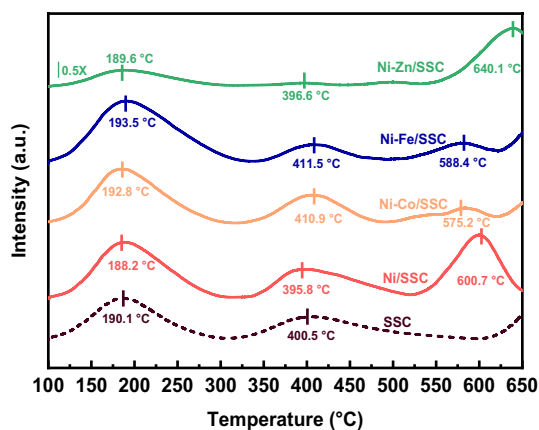


Fig. 7 NH_3 -TPD curves of SSC, Ni/SSC and Ni–M/SSC catalysts. NH_3 -TPD NH_3 -temperature programmed desorption

produces active sites for associative decomposition of NH species, which as a result enhances the NH_3 decomposition performance. After the addition of the second metal (Co, Fe, Zn), Ni–M/SSC presented a similar NH_3 -TPD curve to Ni/SSC. The difference lies in the shift of the strong acidic desorption peak toward lower temperature for Ni–Co/SSC and Ni–Fe/SSC, indicating that the energy barrier of the two catalysts for associative desorption of M–NH bonds is reduced. It can also be observed that the high-temperature desorption peak of Ni–Zn/SSC is shifted right. This may

lead to a decrease in its NH_3 decomposition performance. It has been investigated that the associative decomposition of NH species is the control step of the NH_3 dehydrogenation reaction [41]. Therefore, compared to the Zn promoter, the addition of Co and Fe reduces the energy barrier for the associative decomposition of NH species during the NH_3 decomposition process.

In-situ catalytic NH_3 decomposition

Effect of catalyst type

The in-situ catalytic NH_3 decomposition performance of SSC and its loaded metal catalysts during MSW gasification was investigated at 650 °C under a CO_2 atmosphere. The NH_3 decomposition rate and the corresponding H_2/N_2 proportion in the product gas are shown in Fig. 8. It can be seen from Fig. 8a that both single component Ni/SSC and bimetallic Ni–M catalysts have catalytic activity toward NH_3 decomposition during MSW gasification and their activity is diverse, which is in the order of Ni–Co/SSC > Ni–Zn/SSC > Ni–Fe/SSC > Ni/SSC. Specifically, the NH_3 decomposition rate is 22.48% for Ni/SSC and 40.21%, 27.22%, and 34.54% for Ni–Co/SSC, Ni–Fe/SSC, and Ni–Zn/SSC catalysts, respectively. This demonstrates that the addition of a second metal promotes in-situ NH_3 decomposition, which may be caused by the synergy effect between Ni active sites

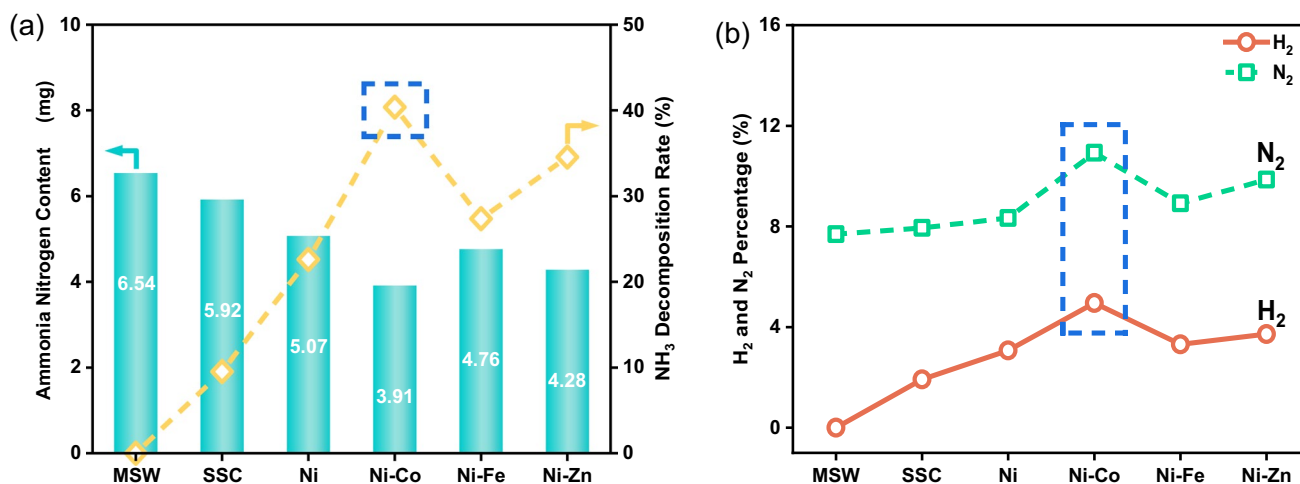


Fig. 8 (a) Ammonia decomposition activity, and (b) hydrogen/nitrogen percentage in product gas over SSC and its supported Ni-based catalysts at 650 °C

and second metal [36]. Besides, the smaller Ni particle size resulting from the addition of second metal indicates a more uniform distribution of Ni active sites, which is also beneficial for enhancing the catalyst activity [37]. Among the three Ni–M bimetallic catalysts, the NH₃ decomposition performance of the Fe and Zn added catalysts is lower than that of the Co added catalyst. The lowest decomposition rate of Ni–Fe/SSC is probably due to the relatively high bonding energy between Fe and N, which occupies active sites for subsequent adsorption and decomposition [42]. The enhanced catalytic performance of Ni–Co/SSC can be explained by its smaller Ni particle size, which facilitates the dispersion of active sites as well as a reduced energy barrier for the associative desorption of NH species during the NH₃ decomposition process.

Interestingly, it was found that the addition of pure SSC also results in a slight decrease in the produced NH₃ amount during MSW gasification, and its NH₃ decomposition rate can reach 9.48%. The unexpected catalytic activity of SSC material may be derived from the residual calcium, iron and other metal elements in the SSC, as proven by some researchers [43]. Moreover, to examine NH₃ decomposition from another perspective, the H₂ and N₂ contents in the gasification gas were tested, and the results are shown in Fig. 8b. It can be seen that the percentages of H₂ and N₂ in the product gas are generally in the same order as the NH₃ decomposition rate in Fig. 8a, among which Ni–Co/SSC has the largest N₂ and H₂ content in product gas. As N₂ and H₂ are the products of NH₃ decomposition, their percentages also indirectly reflect catalyst activity. Furthermore, it can be observed that there is no H₂ produced during pure MSW gasification, which may be consumed by some oxidized components such as CO and CO₂ [44]. Thus, it can be deduced that H₂ production originates entirely from the

decomposition of NH₃ during in-situ catalytic gasification process, while N₂ is co-produced from MSW gasification and NH₃ decomposition.

Effect of reaction temperature

After comparing the performance of the catalysts above, it was found that Ni–Co/SSC exhibited the best NH₃ decomposition activity at 650 °C. Thus, in this section, the effect of temperature on NH₃ decomposition over Ni–Co/SSC was investigated. Fig. 9 shows the effect of reaction temperature on the in-situ NH₃ decomposition ability and H₂/N₂ content in the product gas over the Ni–Co/SSC catalyst. As shown in Fig. 9a, with increasing temperature, the production of NH₃ during the MSW gasification process without catalyst first increases to a peak at 500 °C and then decreases until 700 °C. After adding the Ni–Co/SSC catalyst to the MSW sample for gasification, it was discovered that NH₃ production decreased to different extents. The NH₃ decomposition rate and the corresponding H₂ content generally increase with reaction temperature, which can be explained by the fact that a higher temperature favors the NH₃ decomposition reaction because the reaction is endothermic [45]. In the temperature range of 450–550 °C, the catalyst has almost no activity as proven by the quite small NH₃ decomposition rate (about 2%). This indicates that the in-situ decomposition of NH₃ emitted from MSW gasification at lower temperatures is not feasible, which is possibly caused by the slow reaction kinetics. As the reaction temperature exceeds 550 °C, the decomposition rate of NH₃ gradually increases with increasing temperature and finally reaches a maximum of 43.78% at 700 °C.

From Fig. 9b, it can be observed that without adding the Ni–Co/SSC catalyst, there is still no H₂ produced during

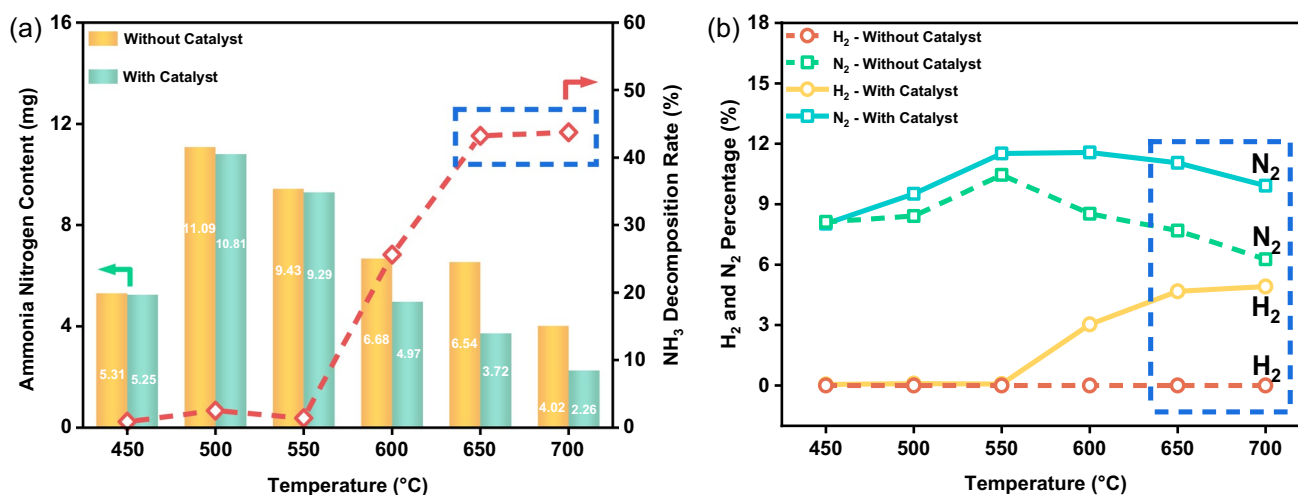


Fig. 9 (a) Ammonia decomposition activity, and (b) hydrogen/nitrogen percentage in product gas under various reaction temperatures over Ni-Co/SSC catalyst

pure MSW gasification even under higher temperatures such as 700 °C. Considering that the gasification medium is CO₂, the generation of H₂ is inhibited in the oxidizing atmosphere [44]. However, N₂ is produced in the whole temperature range and its percentage in product gas increases with reaction temperature at first and then reaches a maximum at 550 °C. After mixing with catalyst, it can be noted that the generation pattern of H₂ is similar to the NH₃ decomposition rate in Fig. 9a, which is because no H₂ is produced from pure MSW gasification and the production of H₂ is entirely derived from the decomposition of NH₃. However, the N₂ generation curve does not fully coincide with the NH₃ decomposition curve, as partial N₂ is derived from MSW gasification. The above results indicate that the reaction temperature has a significant influence on the in-situ NH₃ decomposition activity of the Ni-Co/SSC catalyst, and appropriately increasing the temperature can improve the NH₃ catalytic decomposition performance that finally effectively reduces the emitted NH₃ during the MSW gasification process.

Conclusions

In this article, Ni-M bimetallic catalysts supported on SSC were prepared by co-impregnation method for the in-situ catalytic decomposition of emitted NH₃ from MSW gasification. The catalysts were characterized by XRD, N₂ isothermal adsorption-desorption, SEM and TEM to analyze their phase composition, microscopic parameters and surface morphology, and in-situ catalytic gasification experiments were conducted in a horizontal fixed-bed reactor to investigate their NH₃ decomposition performance and speculate their catalytic decomposition mechanism. The best

Ni-M dual catalyst was screened by comparing the effect of the second metal (Co, Fe, Zn) on the catalytic performance. The results showed that Ni-Co/SSC had the highest NH₃ decomposition rate of 40.21% among the four catalysts at 650 °C. It was found by a series of characterizations that the addition of the second metal effectively reduced the Ni particle size and improved the uniform distribution of the Ni active sites, which promoted the NH₃ decomposition performance of the catalysts. The results of NH₃-TPD suggested that Ni-Co/SSC had the lowest temperature for the strong acid peak. Furthermore, in the temperature range of 450–700 °C, the NH₃ decomposition rate of the Ni-Co/SSC catalyst reaches a maximum of 43.78% at 700 °C, due to the endothermic NH₃ decomposition reaction. This work provides a solution for the control and treatment of NH₃ pollution in the field of solid waste disposal.

Acknowledgements This work was supported by the National Key R&D Program of China (No. 2019YFC1906803) and Key R&D Program of Jiangsu Province (No. BE2021701).

Data availability The data that support the findings of this study are available from the corresponding author upon reasonable request.

Declarations

Conflict of interest The authors declare that they have no conflict of interest.

References

- Yu, J., Sun, L., Wang, B., et al. 2016. Study on the behavior of heavy metals during thermal treatment of municipal solid waste (MSW) components. *Environmental science and pollution research international* 23: 253–265.

2. Cerda, A., Artola, A., Font, X., et al. 2018. Composting of food wastes: status and challenges. *Bioresource Technology* 248: 57–67.
3. Shah, A.V., Srivastava, V.K., Mohanty, S.S., et al. 2021. Municipal solid waste as a sustainable resource for energy production: State-of-the-art review. *Journal of Environmental Chemical Engineering* 9: 105717.
4. Nanda, S., and Berruti, F. 2021. A technical review of bioenergy and resource recovery from municipal solid waste. *Journal of Hazardous Materials* 403: 123970.
5. Wei, J., Li, H., Liu, J., et al. 2022. National and provincial dioxin emissions from municipal solid waste incineration in China. *Science of the Total Environment* 851: 158128.
6. Chuai, X., Yang, Q., Zhang, T., et al. 2022. Speciation and leaching characteristics of heavy metals from municipal solid waste incineration fly ash. *Fuel* 328: 125338.
7. Makarichi, L., Jutidamrongphan, W., and Techato, K.A. 2018. The evolution of waste-to-energy incineration: A review. *Renewable and Sustainable Energy Reviews* 91: 812–821.
8. Yang, Y., Liew, R.K., Tamothran, A.M., et al. 2021. Gasification of refuse-derived fuel from municipal solid waste for energy production: A review. *Environmental Chemistry Letters* 19: 2127–2140.
9. Arena, U. 2012. Process and technological aspects of municipal solid waste gasification review. *Waste Management* 32: 625–639.
10. Lee, D.J. 2022. Gasification of municipal solid waste (MSW) as a cleaner final disposal route: a mini-review. *Bioresour Technology* 344: 126217.
11. Juutilainen, S.J., Simell, P.A., and Krause, A.O.I. 2006. Zirconia: Selective oxidation catalyst for removal of tar and ammonia from biomass gasification gas. *Applied Catalysis B Environmental* 62: 86–92.
12. Xu, C., Donald, J., Byambajav, E., et al. 2010. Recent advances in catalysts for hot-gas removal of tar and NH₃ from biomass gasification. *Fuel* 89: 1784–1795.
13. Wilk, V., Kitzler, H., Koppatz, S., et al. 2011. Gasification of waste wood and bark in a dual fluidized bed steam gasifier. *Biomass Conversion and Biorefinery* 1: 91–97.
14. Jiang, Q., Li, T., He, Y., et al. 2022. Simultaneous removal of hydrogen sulfide and ammonia in the gas phase: A review. *Environmental Chemistry Letters* 20: 1403–1419.
15. Gu, Y., Jin, Z., Zhang, H., et al. 2015. Transition metal nanoparticles dispersed in an alumina matrix as active and stable catalysts for CO_x-free hydrogen production from ammonia. *Journal of Materials Chemistry* 3: 17172–17180.
16. Lamb, K.E., Dolan, M.D., and Kennedy, D.F. 2019. Ammonia for hydrogen storage: A review of catalytic ammonia decomposition and hydrogen separation and purification. *International Journal of Hydrogen Energy* 44: 3580–3593.
17. Le, T.A., Kim, Y., Kim, H.W., et al. 2021. Ru-supported lanthania-ceria composite as an efficient catalyst for CO_x-free H₂ production from ammonia decomposition. *Applied Catalysis B: Environmental* 285: 119831.
18. Lucentini, I., Colli, G.G., Luzzi, C.D., et al. 2021. Catalytic ammonia decomposition over Ni-Ru supported on CeO₂ for hydrogen production: Effect of metal loading and kinetic analysis. *Applied Catalysis B: Environmental* 286: 119896.
19. Pinzon, M., Romero, A., Consuegra, A.D., et al. 2021. Hydrogen production by ammonia decomposition over ruthenium supported on SiC catalyst. *Journal of Industrial and Engineering Chemistry* 94: 326–335.
20. Ji, J., Duan, X., Qian, G., et al. 2013. Fe particles on the tops of carbon nanofibers immobilized on structured carbon microfibers for ammonia decomposition. *Catalysis Today* 216: 254–260.
21. Choi, Y.K., Cho, M.H., and Kim, J.S. 2016. Air gasification of dried sewage sludge in a two-stage gasifier. Part 4: application of additives including Ni-impregnated activated carbon for the production of a tar-free and H₂-rich producer gas with a low NH₃ content. *International Journal of Hydrogen Energy* 41: 1460–1467.
22. Simonsen, S.B., Chakraborty, D., Chorkendorff, I., et al. 2012. Alloyed Ni-Fe nanoparticles as catalysts for NH₃ decomposition. *Applied Catalysis A: General* 447: 22–31.
23. Yin, S., Zhang, Q., Xu, B., et al. 2004. Investigation on the catalysis of CO_x-free hydrogen generation from ammonia. *Journal of Catalysis* 224: 384–396.
24. Lu, A., Nitz, J.J., Comotti, M., et al. 2010. Spatially and size selective synthesis of Fe-based nanoparticles on ordered mesoporous supports as highly active and stable catalysts for ammonia decomposition. *Journal of the American Chemical Society* 132: 14152–14162.
25. Varisli, D., Korkusuz, C., and Dogu, T. 2017. Microwave-assisted ammonia decomposition reaction over iron incorporated mesoporous carbon catalysts. *Applied Catalysis B: Environmental* 201: 370–380.
26. Ren, S., Huang, F., Zheng, J., et al. 2017. Ruthenium supported on nitrogen-doped ordered mesoporous carbon as highly active catalyst for NH₃ decomposition to H₂. *International Journal of Hydrogen Energy* 42: 5105–5113.
27. Zeng, Q., Tang, Nvzhi, Chen, H., et al. 2020. Application research of municipal sludge treatment and disposal technology. *IOP Conference Series: Earth and Environmental Science* 567: 012023.
28. Dai, L., Zhao, W., Zhang, H., et al. 2020. Research progress on adsorption of heavy metals by sewage sludge-based biochar in water. *Environment Engineering* 38: 70–77 ((in Chinese)).
29. Jung, S.Y., Lee, S.J., Park, J.J., et al. 2008. The simultaneous removal of hydrogen sulfide and ammonia over zinc-based dry sorbent supported on alumina. *Separation and Purification Technology* 63: 297–302.
30. Li, G., Zhang, H., Yu, X., et al. 2022. Highly efficient Co/NC catalyst derived from ZIF-67 for hydrogen generation through ammonia decomposition. *International Journal of Hydrogen Energy* 47: 12882–12892.
31. Boisen, A., Dahl, S., Norskov, J., et al. 2005. Why the optimal ammonia synthesis catalyst is not the optimal ammonia decomposition catalyst. *Journal of Catalysis* 230: 309–312.
32. Wu, Z., Li, X., Qin, Y., et al. 2020. Ammonia decomposition over SiO₂-supported Ni-Co bimetallic catalyst for CO_x-free hydrogen generation. *International Journal of Hydrogen Energy* 45: 15263–15269.
33. Wang, F., Zeng, X., Wang, Y., et al. 2015. Investigation on in/ex-situ coal char gasification kinetics in a micro fluidized bed reactor. *Journal of Fuel Chemistry and Technology* 43: 393–401 ((in Chinese)).
34. Hashemnejad, S.M., and Parvari, M. 2011. Deactivation and regeneration of nickel-based catalysts for steam-methane reforming. *Chinese Journal of Catalysis* 32: 273–279.
35. Wu, H., Cao, A. 2013. Preparation and adding methods of Nessler's Reagent having effects on determination of water quality ammonia nitrogen. *Advanced Materials Research* 726-731: 1362–1366
36. Khan, W.U., Alasiri, H.S., Ali, S.A. et al. 2022. Recent advances in bimetallic catalysts for hydrogen production from ammonia. *Chemical Record* 22 (7): e202200030.
37. Fu, E., Qiu, Y., Lu, H., et al. 2021. Enhanced NH₃ decomposition for H₂ production over bimetallic M(M=Co, Fe, Cu)/Ni/Al₂O₃. *Fuel Processing Technology* 221: 106945.
38. Dong, X., Jin, B., Cao, S., et al. 2020. CO_x co-methanation over coal combustion fly ash supported Ni-Re bimetallic catalyst: transformation from hazardous to high value-added products. *Journal of Hazardous Materials* 396: 122668.
39. Hu, X., Wang, W., Jin, Z., et al. 2019. Transition metal nanoparticles supported La-promoted MgO as catalysts for hydrogen

- production via catalytic decomposition of ammonia. *Journal of Energy Chemistry* 38: 41–49.
40. Qiu, J., Peng, Y., Tang, M., et al. 2022. Solvothermal preparation of Mn-based catalysts for simultaneous removal of 1,2-dichlorobenzene and furan. *Waste Disposal & Sustainable Energy* 4: 105–116.
 41. Takahashi, A., and Fujitani, T. 2016. Kinetic analysis of decomposition of ammonia over nickel and ruthenium catalysts. *Journal of Chemical Engineering of Japan* 49: 22–28.
 42. Yeo, S.C., Han, S.S., and Lee, H.M. 2014. Mechanistic investigation of the catalytic decomposition of ammonia (NH₃) on an Fe (100) Surface: A DFT Study. *Journal of Physical Chemistry C* 118: 5309–5316.
 43. Yi, K., Liu, H., Wang, J., et al. 2019. The adsorption and transformation of SO₂, H₂S and NH₃ by using sludge gasification ash: effects of Fenton oxidation and CaO pre-conditioning. *Chemical Engineering Journal* 360: 1498–1508.
 44. Mauerhofer, A.M., Fuchs, J., Muller, S., et al. 2019. CO₂ gasification in a dual fluidized bed reactor system: impact on the product gas composition. *Fuel* 253: 1605–1616.
 45. Qiu, S., Ren, T., and Li, J. 2018. The latest advances in the modified catalysts for hydrogen production from ammonia decomposition. *Chemical Industry and Engineering Progress* 37: 1001–1007 ((in Chinese)).

Publisher's Note Springer Nature remains neutral with regard to jurisdictional claims in published maps and institutional affiliations.

Springer Nature or its licensor (e.g. a society or other partner) holds exclusive rights to this article under a publishing agreement with the author(s) or other rightsholder(s); author self-archiving of the accepted manuscript version of this article is solely governed by the terms of such publishing agreement and applicable law.